

Reconfigurable Intelligent Surfaces for Energy Efficiency in Wireless Communication

Chongwen Huang, Alessio Zappone, *Senior Member, IEEE*,

George C. Alexandropoulos, *Senior Member, IEEE*,

Mérouane Debbah, *Fellow, IEEE*, and Chau Yuen, *Senior Member, IEEE*

Abstract

The adoption of a Reconfigurable Intelligent Surface (RIS) for downlink multi-user communication from a multi-antenna base station is investigated in this paper. We develop energy-efficient designs for both the transmit power allocation and the phase shifts of the surface reflecting elements, subject to individual link budget guarantees for the mobile users. This leads to non-convex design optimization problems for which to tackle we propose two computationally affordable approaches, capitalizing on alternating maximization, gradient descent search, and sequential fractional programming. Specifically, one algorithm employs gradient descent for obtaining the RIS phase coefficients, and fractional programming for optimal transmit power allocation. Instead, the second algorithm employs sequential fractional programming for the optimization of the RIS phase shifts. In addition, a realistic power consumption model for RIS-based systems is presented, and the performance of the proposed methods is analyzed in a realistic outdoor environment. In particular, our results show that the proposed RIS-based resource allocation methods are able to provide up to 300% higher energy efficiency, in comparison with the use of regular multi-antenna amplify-and-forward relaying.

Index Terms

Part of this work has been presented in *IEEE ICASSP*, Calgary, Canada, 14–20 April 2018 [1].

C. Huang and C. Yuen are with the Singapore University of Technology and Design, 487372 Singapore. (emails: chongwen_huang@mymail.sutd.edu.sg, yuenchau@sutd.edu.sg)

A. Zappone and M. Debbah are with CentraleSupélec, University Paris-Saclay, 91192 Gif-sur-Yvette, France. M. Debbah is also with the Mathematical and Algorithmic Sciences Lab, Paris Research Center, Huawei Technologies France SASU, 92100 Boulogne-Billancourt, France. (emails: alessio.zappone@l2s.centralesupelec.fr, merouane.debbah@huawei.com)

G. C. Alexandropoulos was with the Mathematical and Algorithmic Sciences Lab, Paris Research Center, Huawei Technologies France SASU, 92100 Boulogne-Billancourt, France. He is now with the Department of Informatics and Telecommunications, National and Kapodistrian University of Athens, Panepistimiopolis Ilissia, 15784 Athens, Greece. (e-mail: alexandg@di.uoa.gr)

Reconfigurable intelligent surfaces, multi-user MIMO, energy efficiency, phase shift, non-convex optimization, alternating maximization, gradient descent, sequential fractional programming.

I. INTRODUCTION

The highly demanding data rate requirements of emerging and future wireless networks (5-th Generation (5G) and beyond) have raised serious concerns on their energy consumption [2], [3]. These networks are anticipated to connect over 50 billions of wireless capability devices by 2020 [4] via dense deployments of multi-antenna base stations and access points [5]–[7]. As a consequence, the bit-per-Joule Energy Efficiency (EE) has emerged as a key performance indicator to ensure green and sustainable wireless networks [2], [3], [8], and several energy efficient wireless solutions have been proposed. A survey on the different approaches to implement energy efficient 5G wireless networks has recently appeared in [9]. Therein, the authors conclude that the energy challenge can be conquered only by the joint use of multiple approaches ranging from the use of renewable energy sources, energy efficient hardware components and relevant deployment techniques, as well as green resource allocation and transceiver signal processing algorithms. The issue of radio resource allocation for EE maximization in wireless networks is addressed in detail in [10], where the related mathematical tools are discussed. In [11]–[14] it is established that deploying a massive number of antennas can bring substantial energy-efficient benefits.

Among the candidate transceiver approaches [15]–[18] for green communication, a recent emerging hardware technology with increased potential for significant energy consumption reductions is the so-called reconfigurable intelligent surface (RIS) [14], [19]–[23]. A RIS is a meta-surface equipped with integrated electronic circuits that can be programmed to alter an incoming electromagnetic field in a customizable way. It consists of a single- or few-layer stack of planar structures that can be readily fabricated using lithography and nano-printing methods. Each RIS unit is implemented by reflect-arrays that employ varactor diodes or other Micro-Electrical-Mechanical Systems, and whose resonant frequency is electronically controlled [15], [21], [24]–[28]. The RIS units operating on the incoming field can be distributed over the metasurface with continuity [14], [19], [20], [29] or in discrete positions [15], [22], [23], [30].

Regardless of the specific implementation, what makes the RIS technology attractive from an energy consumption standpoint, is the possibility of amplifying and forwarding the incoming signal without employing any power amplifier, but rather by suitably designing the phase shifts

applied by each reflecting element, in order to constructively combine each reflected signal. Clearly, since no amplifier is used, a RIS will consume much less energy than a regular Amplify-and-Forward (AF) relay transceiver. Moreover, RIS structures can be easily integrated in the communication environment, since their very low hardware footprint allows for their easy deployment into buildings facades, room and factory ceilings, laptop cases, up to being integrated into human clothing [18], [31]. On the other hand, the lack of an amplifier implies that the gain of a RIS will be lower than what can be achieved by a traditional AF relay with a number of antennas equal to the number of reflecting elements of the RIS. Thus, as far as EE is concerned, it is not clear if a RIS-based system is more convenient than traditional AF relay-based systems [32]–[35]. This work aims at answering this question, showing that by properly designing the phase shifts applied by the RIS leads to higher EE than that of a communication system based on traditional AF relays.

Available works on RIS-based communication system have mainly focused on the rate performance of RIS in indoor environments. In [36], a $0.4m^2$ and $1.5mm$ thickness planar metasurface consisting of 102 controllable electromagnetic unit cells and operating at 2.47GHz was designed. Each unit cell is a rectangular patch sitting on a ground plane [37] and offering binary phase modulation. The metasurface was deployed as a spatial microwave modulator in a typical office room, and was demonstrated that it can passively increase the received signal power by an order of magnitude, or completely null it. Integrating each unit cell with one PIN diode in [30], a programmable metasurface with dynamic polarization, scattering, and focusing control was designed. The presented experiments demonstrated various controllable electromagnetic phenomena, including anomalous reflection and diffusion, as well as beamforming [20], [38]. A detailed analysis on the information transfer from multiple users to a RIS with active elements was carried out in [14], while [26] showed that a reflectarray can effectively achieve amplification gains, while at the same time cancel interference. In this work, the results were also corroborated by measurements carried out on an office testbed. The role of RIS in improving indoor coverage was also analyzed in [39], [40]. Very recently, [27] experimented on the incorporation of a smart reflectarray in an IEEE 802.11ad network operating in the unlicensed 60GHz frequency band. In [21] the adoption of intelligent metasurfaces for actively reprogramming communication environments is envisioned, and its advantages in terms of coverage, energy saving, and security are discussed.

In this work, we consider the downlink of an outdoor cellular network in which a multiple-

antenna BS reaches the single-antenna mobile users through a RIS that forwards a suitably phase-shifted version of the transmitted signal. A discrete RIS implementation is adopted, in which a finite number of reflecting units are equipped on the intelligent surface. The contributions of this paper are summarized as follows.

- We develop a realistic RIS power consumption model that is based on the number of deployed reflector units and their phase resolution capability. This allows us to formulate the EE maximization problem to optimize the RIS phase shifts and the downlink transmit powers under maximum power and minimum Quality of Service (QoS) constraints.
- We develop two novel low complexity, and provably convergent, optimization algorithms to tackle the EE maximization problem that account for the unit-modulus constraint of the RIS phase shifts, that is not to be enforced in the design of traditional relay systems. The proposed algorithms exploit the frameworks of alternating maximization, sequential fractional programming, and conjugate gradient search.
- We numerically evaluate the performance of the proposed algorithms in a realistic outdoor scenario, while all previous works about RIS have focused on indoor settings. Our results indicate that the proposed algorithms are indeed able to grant higher EE performance than that obtained by a traditional relay-assisted communication system.

The remainder of this paper is organized as follows. In Section II, the multi-user MISO system assisted by reconfigurable RIS structures is described and the targeted EE maximization problem is formulated. The two derived algorithms for the EE maximization design are presented in Section III, and extensive numerically evaluated results are provided in Section IV. Finally, concluding remarks and future research directions are drawn in Section V.

Notation: a is a scalar, \mathbf{a} is a vector, and \mathbf{A} is a matrix. \mathbf{A}^T , \mathbf{A}^H , \mathbf{A}^{-1} , \mathbf{A}^+ , and $\|\mathbf{A}\|_F$ denote transpose, Hermitian (conjugate transpose), inverse, pseudo-inverse, and Frobenius norm of \mathbf{A} , respectively. $\text{Re}(\cdot)$, $\text{Im}(\cdot)$, $|\cdot|$, $(\cdot)^*$ and $\arg(\cdot)$ denote the real part, imaginary part, modulus, conjugate and the angle of a complex number, respectively. $\text{tr}(\cdot)$ denotes the trace of a matrix and \mathbf{I}_n (with $n \geq 2$) is the $n \times n$ identity matrix. $\mathbf{A} \circ \mathbf{B}$ and $\mathbf{A} \otimes \mathbf{B}$ denote the Hadamard and Kronecker products of \mathbf{A} and \mathbf{B} , respectively, while $\text{vec}(\mathbf{A})$ is a vector stacking all the columns of \mathbf{A} . $\text{diag}(\mathbf{a})$ is a diagonal matrix with the entries of \mathbf{a} on its main diagonal. $\mathbf{A} \succeq \mathbf{B}$ means that $\mathbf{A} - \mathbf{B}$ is positive semidefinite. Notation $x \sim \mathcal{CN}(0, \sigma^2)$ means that random variable x is complex circularly symmetric Gaussian with zero mean and variance σ^2 , whereas $E[x]$

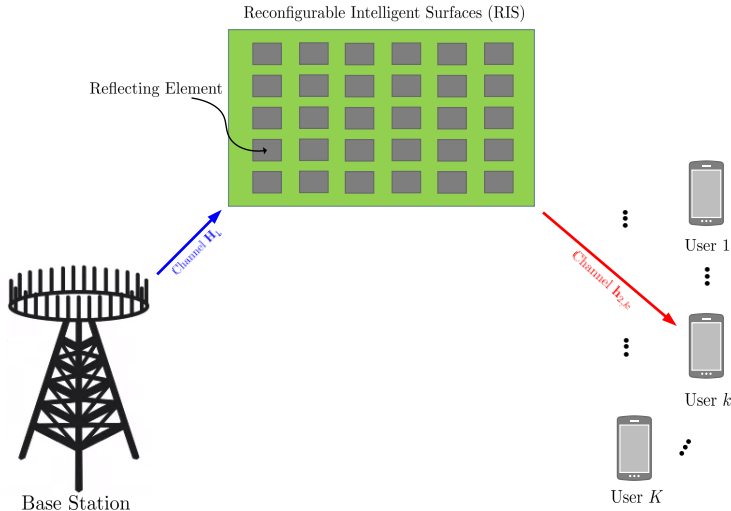


Figure 1. The considered RIS-based multi-user MISO system comprising of a M -antenna base station simultaneously serving in the downlink K single-antenna users. RIS is assumed to be attached to a surrounding building's facade, and the transmit signal propagates to the users via the assistance of RIS that is capable of reconfigurable behavior.

denotes x 's expected value. \mathbb{R} and \mathbb{C} denote the complex and real number sets, respectively, and $j \triangleq \sqrt{-1}$ is the imaginary unit.

II. SYSTEM MODEL

In this section, we describe the signal model for the considered RIS-based downlink multi-user MISO system, and then develop a model for the system total power consumption, which accounts for the energy consumption at the RIS. This section also describes the problem formulation for the joint design of the users' transmit powers and RIS phase shifts.

A. Signal Model

Consider the downlink communication between a BS equipped with M antenna elements and K single-antenna mobile users. We assume that this communication takes place via a RIS with N reflecting elements deployed on the facade of a building existing in the vicinity of both communication ends, as illustrated in Fig. 1. The direct signal path between the BS and the mobile users is neglected due to unfavorable propagation conditions.

Then, the discrete-time signal received at mobile user k , with $k = 1, 2, \dots, K$, is written as

$$y_k = \mathbf{h}_{2,k} \mathbf{\Phi} \mathbf{H}_1 \mathbf{x} + w_k \quad (1)$$

where $\mathbf{h}_{2,k} \in \mathbb{C}^{1 \times N}$ denotes the channel vector between the RIS and user k , $\mathbf{H}_1 \in \mathbb{C}^{N \times M}$ denotes the channel matrix between the BS and the RIS, $\Phi \triangleq \text{diag}[\phi_1, \phi_2, \dots, \phi_N]$ is a diagonal matrix accounting for the effective phase shifts applied by all RIS reflecting elements, where $\phi_n = e^{j\theta_n} \forall n = 1, 2, \dots, N$, while $w_k \sim \mathcal{CN}(0, \sigma^2)$ models the thermal noise power at receiver k .

Finally, $\mathbf{x} \triangleq \sum_{k=1}^K \sqrt{p_k} \mathbf{g}_k s_k$ denotes the transmitted signal with p_k , s_k , and $\mathbf{g}_k \in \mathbb{C}^{M \times 1}$ representing the transmit power, unit-power complex valued information symbol chosen from a discrete constellation set, and precoding vector, respectively, intended for the k -th mobile user. The power of the transmit signal from the multi-antenna BS is subject to the maximum transmit power constraint:

$$E[|\mathbf{x}|^2] = \text{tr}(\mathbf{P}\mathbf{G}^H\mathbf{G}) \leq P_{\max}, \quad (2)$$

wherein $\mathbf{G} \triangleq [\mathbf{g}_1, \mathbf{g}_2, \dots, \mathbf{g}_K] \in \mathbb{C}^{M \times K}$, $\mathbf{P} \triangleq \text{diag}[p_1, \dots, p_K] \in \mathbb{R}^{K \times K}$.

As seen from (1), the reflecting surface is modeled as a scatterer with reconfigurable characteristics. It effectively applies the phase shifting operation described by Φ to the impinging information bearing signal expressed by $\mathbf{H}_1\mathbf{x}$. Thus, a RIS operates in way that resembles an AF relay, with the crucial difference that no power amplifier is present in a RIS. As a result, unlike what happens in AF relaying, each RIS coefficient is constrained to have unit modulus. Moreover, a RIS does not perform any decoding, and/or digitalization operation, operating instead directly on the RF incoming signal [15], [26], [27], [39], [40]. As a result, a RIS is anticipated to require a much lower energy consumption than a traditional AF relay, requiring only a limited, static power supply.

Based on (1), the Signal-to-Interference-plus-Noise Ratio (SINR) experienced at the k -th mobile user is obtained as

$$\gamma_k \triangleq \frac{p_k |\mathbf{h}_{2,k} \Phi \mathbf{H}_1 \mathbf{g}_k|^2}{\sum_{i=1, i \neq k}^K p_i |\mathbf{h}_{2,k} \Phi \mathbf{H}_1 \mathbf{g}_i|^2 + \sigma^2}. \quad (3)$$

Then, based on (3), the system Spectral Efficiency (SE) in bps/Hz is given by

$$\mathcal{R} \triangleq \sum_{k=1}^K \log_2(1 + \gamma_k). \quad (4)$$

B. Total Power Consumption Model

The total power dissipated to operate the considered RIS-based system is composed of the BS transmit power, as well as the hardware static power consumed in the BS, mobile user terminals,

and RIS. In particular, it should be stressed that the RIS does not consume any transmit power, since its reflectors are passive elements that do not directly alter the magnitude of the incoming signal. Any amplification gain provided by the RIS is obtained through a suitable adjustment of the phase shifts of the reflecting elements so as to recombine the reflected signals with a phase coherence. As previously mentioned, this is a significant difference compared to AF relay architectures [41], which instead rely on dedicated power amplifier to achieve amplification gains.

Putting all above together, the power consumption of the k -th wireless link between BS and the k -th mobile user can be expressed as

$$\mathcal{P}_k \triangleq \xi p_k + P_{\text{UE},k} + P_{\text{BS}} + P_{\text{RIS}}, \quad (5)$$

wherein $\xi \triangleq \nu^{-1}$ with ν being the efficiency of the transmit power amplifier, $P_{\text{UE},k}$ is the hardware static power dissipated by the k -th user equipment, while P_{BS} and P_{RIS} denote the total hardware static power consumption at BS and RIS, respectively. We should remark that the two underlying assumptions in (5) are: *i*) the transmit amplifier operates in its linear region; and *ii*) the circuit power P_c does not depend on the communication rate. Both assumptions are met in typical wireless communication systems, which are operated so as to ensure that the amplifiers operate in the linear region of their transfer function, and in which the hardware-dissipated power can be approximated by a constant power offset.

The RIS power consumption depends on the type and the resolution of its individual reflecting elements that effectively perform phase shifting on the impinging signal. Typical power consumption values of each phase shifter are 1.5, 4.5, 6, and 7.8mW for 3-, 4-, 5-, and 6-bit resolution phase shifting [18], [42]–[44]. Therefore, the power dissipated at an intelligent surface with N identical reflecting elements can be written as $P_{\text{RIS}} = NP_n(b)$, where $P_n(b)$ denotes the power consumption of each phase shifter having b -bit resolution. Using the latter definitions, the total amount of power needed to operate the RIS-based downlink multi-user MISO system is given by

$$\mathcal{P}_{\text{total}} = \sum_{k=1}^K (\xi p_k + P_{\text{UE},k}) + P_{\text{BS}} + NP_n(b). \quad (6)$$

In the following, the power model in (6) will be considered as the denominator of the energy efficiency function, even though the optimization of the number of quantization bits b will not be considered, and left for thorough investigation in future work. Some preliminary results on the optimization of b have appeared in [18].

C. Design Problem Formulation

We are interested in the joint design of the transmit powers for all users, included in $\mathbf{P} = \text{diag}[p_1, p_2, \dots, p_K]$, and the values for the RIS elements, appearing in the diagonal of $\Phi = \text{diag}[\phi_1, \phi_2, \dots, \phi_N]$, that jointly maximize the bit-per-Joule EE performance for the considered RIS-based system. This performance is defined as the ratio between the system achievable sum rate in bps and the total power consumption in Joule, i.e., $\eta_{\text{EE}} \triangleq \text{BWR}/\mathcal{P}_{\text{total}}$ with BW being the transmission bandwidth, and can be obtained using (4) and (6) as

$$\eta_{\text{EE}} = \frac{\text{BW} \sum_{k=1}^K \log_2(1 + \gamma_k)}{\xi \sum_{k=1}^K p_k + P_{\text{BS}} + K P_{\text{UE}} + N P_n(b)}. \quad (7)$$

The EE maximization will be carried out enforcing maximum power constraints as well as individual QoS requirements for all K mobile users. To make the targeted problem more tractable, we assume that: *i*) the reflectors phase shifting resolution is infinite, i.e., $2^b \gg 1$; and *ii*) all involved channels are perfectly known at BS that employs Zero-Forcing (ZF) transmission, which is known to be optimal in the high-SINR regime¹ [45], [46]. To this end, it is assumed that the BS perfectly knows all communication channels $\mathbf{h}_{2,k} \forall k = 1, 2, \dots, K$ and \mathbf{H}_1 , which can be acquired by the methods described in e.g. [47], [48].

The ZF precoding matrix is given by $\mathbf{G} = (\mathbf{H}_2 \Phi \mathbf{H}_1)^+$, where $\mathbf{H}_2 \triangleq [\mathbf{h}_{2,1}^T, \mathbf{h}_{2,2}^T, \dots, \mathbf{h}_{2,K}^T]^T \in \mathbb{C}^{K \times N}$. Substituting this \mathbf{G} in (3), the considered EE maximization problem is expressed as follows:

$$\max_{\Phi, \mathbf{P}} \frac{\sum_{k=1}^K \log_2(1 + p_k \sigma^{-2})}{\xi \sum_{k=1}^K p_k + P_{\text{BS}} + K P_{\text{UE}} + N P_n(b)} \quad (8a)$$

$$\text{s.t. } \log_2(1 + p_k \sigma^{-2}) \geq R_{\min,k} \quad \forall k = 1, 2, \dots, K, \quad (8b)$$

$$\text{tr}((\mathbf{H}_2 \Phi \mathbf{H}_1)^+ \mathbf{P} (\mathbf{H}_2 \Phi \mathbf{H}_1)^{+H}) \leq P_{\max}, \quad (8c)$$

$$|\phi_n| = 1 \quad \forall n = 1, 2, \dots, N, \quad (8d)$$

where $R_{\min,k}$ denotes the individual QoS constraint of the k -th user. Also, constraint (8c) ensures that the BS transmit power is kept below the maximum feasible threshold P_{\max} , while constraint (8d) accounts for the fact that each RIS reflecting element can only provide a phase shift, without amplifying the incoming signal.

¹It is well-known that in general the optimal linear receive structure is the LMMSE filter. However, this has the drawback of not suppressing the multi-user interference, which would significantly complicate the resource allocation phase.

The optimization problem (8) is non-convex, and is made particularly challenging by the presence of Φ . In the sequel, we present two computationally efficient approaches to tackle (8).

III. ENERGY EFFICIENCY MAXIMIZATION

Solving the optimization problem described in (8) is challenging mainly due to the constraints (8c) and (8d). In order to develop a tractable algorithm for the design parameters, a convenient approach is to employ the alternating optimization technique [49] to separately and iteratively solve for \mathbf{P} and Φ . In particular, we first solve for Φ given a fixed \mathbf{P} , and then find the optimum \mathbf{P} when Φ is fixed. Iterating this process improves the EE value at each iteration step, and must eventually converge in the optimum value of the objective, since (8a) is upper-bounded on the feasible set. In the rest of this section, the optimization with respect to Φ for fixed \mathbf{P} , and with respect to \mathbf{P} for fixed Φ will be treated separately.

A. Optimization with respect to the RIS Elements Values Φ

For a fixed transmit power allocation matrix \mathbf{P} , the design problem (8) becomes the following feasibility test:

$$\max_{\Phi} C_o \tag{9a}$$

$$\text{s.t. } \text{tr}((\mathbf{H}_2 \Phi \mathbf{H}_1)^+ \mathbf{P} (\mathbf{H}_2 \Phi \mathbf{H}_1)^{+H}) \leq P_{\max}, \tag{9b}$$

$$|\phi_n| = 1 \quad \forall n = 1, 2, \dots, N, \tag{9c}$$

wherein C_o denotes any constant number. Since the power allocation matrix \mathbf{P} is fixed, the objective can be reduced as a constant-value objective function C_o under the constraints (9b) and (9c). The challenge in solving problem (9) lies in the fact that its objective is non-differentiable and that the feasible set is not convex. To proceed further, we observe that (9) is feasible if and only if the solution of the following optimization problem:

$$\min_{\Phi} \text{tr}((\mathbf{H}_2 \Phi \mathbf{H}_1)^+ \mathbf{P} (\mathbf{H}_2 \Phi \mathbf{H}_1)^{+H}) \tag{10a}$$

$$\text{s.t. } |\phi_n| = 1 \quad \forall n = 1, 2, \dots, N \tag{10b}$$

is such that the objective can be made lower than P_{\max} .

Let us define $\Theta \triangleq \text{diag}[\theta_1, \theta_2, \dots, \theta_N]$ and then express Φ as the following function of Θ (recall that $\phi_n = e^{j\theta_n} \forall n = 1, 2, \dots, N$): $\Phi(\Theta) = \text{diag}[e^{j\theta_1}, e^{j\theta_2}, \dots, e^{j\theta_N}]$. Using these definitions, problem (10) can be reformulated as the following unconstrained problem:

$$\min_{\Theta} \mathcal{F}(\Phi(\Theta)) \triangleq \text{tr}((\mathbf{H}_2 \Phi(\Theta) \mathbf{H}_1)^+ \mathbf{P} (\mathbf{H}_2 \Phi(\Theta) \mathbf{H}_1)^{+H}). \quad (11)$$

By expressing the power allocation matrix \mathbf{P} as $\mathbf{P} = \mathbf{Q}\mathbf{Q}^T$ with $\mathbf{Q} \triangleq \sqrt{\mathbf{P}}$, we observe that the objective function in (11) can be rewritten as

$$\begin{aligned} \mathcal{F}(\Phi(\Theta)) &= \text{tr}((\mathbf{H}_2 \Phi(\Theta) \mathbf{H}_1)^+ \mathbf{P} (\mathbf{H}_2 \Phi(\Theta) \mathbf{H}_1)^{+H}) \\ &= \text{tr}((\mathbf{Q}^{-1} \mathbf{H}_2 \Phi(\Theta) \mathbf{H}_1)^+ (\mathbf{Q}^{-1} \mathbf{H}_2 \Phi(\Theta) \mathbf{H}_1)^{+H}) \\ &\stackrel{a}{=} \text{tr}((\overline{\mathbf{H}}_2 \Phi(\Theta) \mathbf{H}_1)^+ (\overline{\mathbf{H}}_2 \Phi(\Theta) \mathbf{H}_1)^{+H}) \stackrel{b}{=} \|\mathbf{H}_1^+ \Phi^{-1}(\Theta) \overline{\mathbf{H}}_2^+\|_F^2 \\ &\stackrel{c}{=} \|\text{vec}(\mathbf{H}_1^+ \Phi^{-1}(\Theta) \overline{\mathbf{H}}_2^+)\|^2 = \|(\overline{\mathbf{H}}_2^{+H} \otimes \mathbf{H}_1^+) \text{vec}(\Phi^{-1}(\Theta))\|^2 \\ &= \text{vec}(\Phi^{-1}(\Theta))^H (\overline{\mathbf{H}}_2^{+H} \otimes \mathbf{H}_1^+)^H (\overline{\mathbf{H}}_2^{+H} \otimes \mathbf{H}_1^+) \text{vec}(\Phi^{-1}(\Theta)). \end{aligned} \quad (12)$$

In the latter expression, we have used the definition $\overline{\mathbf{H}}_2 \triangleq \mathbf{Q}^{-1} \mathbf{H}_2$ in step (a), whereas steps (b) follows from the properties of the Frobenius norm and Pseudo-inverse law of a matrix product,² and (c) follows from the vectorization operator, respectively. While the alternative expression in (12) does not lead to a convex problem formulation, it lends itself to being handled by the two efficient approaches to be described in the next two subsections.

1) *Gradient Descent Approach:* The optimization problem $\min_{\Theta} \mathcal{F}(\Phi(\Theta))$ using (12) is an unconstrained problem, hence, we can employ gradient search to monotonically decrease its objective, eventually converging to a stationary point. To begin with, we first define the matrices:

$$\mathbf{A} \triangleq (\overline{\mathbf{H}}_2^{+H} \otimes \mathbf{H}_1^+)^H (\overline{\mathbf{H}}_2^{+H} \otimes \mathbf{H}_1^+) \in \mathbb{C}^{N^2 \times N^2}, \quad (13)$$

$$\mathbf{y} \triangleq \text{vec}(\Phi^{-1}(\Theta)) \in \mathbb{C}^{N^2 \times 1}, \quad (14)$$

which help us to express (12) as $\mathcal{F}(\Phi(\Theta)) = \mathbf{y}^H \mathbf{A} \mathbf{y}$. To compute the gradient of $\mathcal{F}(\Phi(\Theta))$ with respect to Θ , i.e., $\nabla_{\Theta}(\mathbf{y}^H \mathbf{A} \mathbf{y})$, we expand $\mathbf{y}^H \mathbf{A} \mathbf{y}$ using (14), which, upon exploiting the fact that $\mathbf{A} = \mathbf{A}^H$, leads to:

$$\mathbf{y}^H \mathbf{A} \mathbf{y} = \sum_{n=1}^N a_{\ell(n), \ell(n)} + 2\Re \left\{ \sum_{n=1}^N \sum_{m>n}^N a_{\ell(n), \ell(m)} e^{j(\theta_n - \theta_m)} \right\}, \quad (15)$$

² Assuming $K \geq N$ and $M \geq N$, and exploiting the fact that \mathbf{H}_1 and \mathbf{H}_2 are realizations of random matrices with i.i.d. entries, it holds that $\overline{\mathbf{H}}_2$ has full column rank and $\Phi(\Theta) \mathbf{H}_1$ has full row rank. Thus, $(\overline{\mathbf{H}}_2 \Phi \mathbf{H}_1)^+ = \mathbf{H}_1^+ \Phi^{-1} \overline{\mathbf{H}}_2^+$.

where $\ell(n)$ is the index map $\ell(n) = (n-1)N+n$, for all $n = 1, \dots, N$, and $a_{\ell(n),\ell(m)}$ denotes the $(\ell(n), \ell(m))$ -th element of \mathbf{A} . Then, the derivative of $\mathbf{y}^H \mathbf{A} \mathbf{y}$ with respect to $\theta_i \forall i = 1, 2, \dots, N$ can be computed as

$$\frac{\partial(\mathbf{y}^H \mathbf{A} \mathbf{y})}{\partial \theta_i} = 2\Re \left\{ j e^{j\theta_i} \sum_{m>i}^N a_{\ell(i),\ell(m)} e^{-j\theta_m} - j e^{-j\theta_i} \sum_{n<i}^N a_{\ell(n),\ell(i)} e^{j\theta_n} \right\}. \quad (16)$$

Next, a suitable step size for the gradient descent needs to be computed. To this end, denote by $\text{vec}(\Theta)^t$ the phase of \mathbf{y} at iteration t , and by \mathbf{d}^t the adopted descent direction at iteration t . Then, the next iteration point is given by

$$\text{vec}(\Theta)^{(t+1)} = \text{vec}(\Theta)^{(t)} + \mu \mathbf{d}^{(t)}, \quad (17)$$

$$\mathbf{y}^{(t+1)} = e^{j\text{vec}(\Theta)^{(t+1)}} \circ \text{vec}(\mathbf{I}_N) = \mathbf{y}^{(t)} \circ e^{j\mu \mathbf{d}^{(t)}}, \quad (18)$$

where $\mu > 0$ is the step size. In order to find a suitable step size, we need to solve the following minimization problem:

$$\min_{\mu>0} h(\mu) \triangleq (\mathbf{y}^{(t+1)})^H \mathbf{A} \mathbf{y}^{(t+1)}, \quad (19)$$

To this end, we expand $h(\mu)$ by plugging (18) into (15), which yields

$$h(\mu) = \sum_{n=1}^N a_{\ell(n),\ell(n)} + 2\Re \left\{ \sum_{n=1}^N \sum_{m>n}^N a_{\ell(n),\ell(m)} e^{j(\theta_n^{(t)} - \theta_m^{(t)})} e^{j\mu(d_m^{(t)} - d_n^{(t)})} \right\}, \quad (20)$$

wherein $d_n^{(t)}$ is the n -th element of $\mathbf{d}^{(t)}$. Then, $h(\mu)$ can be minimized by means of a line search over $\mu > 0$. On the other hand, aiming at a complexity reduction, one can consider a quadratic approximation of (20) by considering the second-order Taylor expansion of the term $e^{j\mu(d_m^{(t)} - d_n^{(t)})}$ around $\mu = 0$, which yields the following approximation of $h(\mu)$

$$\hat{h}(\mu) = \sum_{n=1}^N a_{\ell(n),\ell(n)} + 2\Re \left\{ \sum_{n=1}^N \sum_{m>n}^N a_{\ell(n),\ell(m)} e^{j(\theta_n^{(t)} - \theta_m^{(t)})} \left(1 + j\mu(d_m^{(t)} - d_n^{(t)}) + \frac{(j\mu(d_m^{(t)} - d_n^{(t)}))^2}{2} \right) \right\} \quad (21)$$

Thus, denoting by z_0, z_1, z_2 the constant, linear, and quadratic term in (21), respectively, we obtain the simple approximation

$$\hat{h}(\mu) = z_0 + z_1 \mu - z_2 \mu^2, \quad (22)$$

which admits the closed-form maximizer $\mu^* = z_1/(2z_2)$ if³ $z_1 \geq 0, z_2 > 0$.

³Traditional line search can be used if these conditions do not hold.

At this point, equipped with an expression for the gradient of the objective function $\mathcal{F}(\Phi(\Theta))$ as well as a simple way to obtain the step-size, we employ the Polak-Ribiere-Polyak conjugate gradient algorithm to update the descent direction using the following formula [50], [51]:

$$\mathbf{d}^{(t+1)} = -\mathbf{q}^{(t+1)} + \frac{(\mathbf{q}^{(t+1)} - \mathbf{q}^{(t)})^T \mathbf{q}^{(t+1)}}{\|\mathbf{q}^{(t)}\|^2} \mathbf{d}^{(t)}, \quad (23)$$

where $\mathbf{q}^{(t)} \triangleq \nabla_{\Theta} ((\mathbf{y}^{(t)})^H \mathbf{A} \mathbf{y}^{(t)})$. It should be mentioned that, in case the step size is computed based on the approximate function $\hat{h}(\mu)$ in (22), it is not guaranteed that $\mathbf{d}^{(t)}$ is a descent direction. Thus, in order to guarantee that at each iteration t of the gradient search we obtain a descent direction, we consider the following modified direction update rule:

$$\mathbf{d}^{(t+1)} = \begin{cases} \mathbf{d}^{(t+1)}, & (\mathbf{q}^{(t+1)})^T \mathbf{d}^{(t+1)} < 0 \\ -\mathbf{q}^{(t+1)}, & (\mathbf{q}^{(t+1)})^T \mathbf{d}^{(t+1)} \geq 0 \end{cases}.$$

2) *Sequential Fractional Programming*: By substituting (12) into (10), the optimization problem with respect to Φ for given \mathbf{P} can be rewritten as

$$\min_{\Phi} \text{vec}(\Phi^{-1})^H \mathbf{A} \text{vec}(\Phi^{-1}) \quad (24a)$$

$$\text{s.t. } |\phi_n| = 1 \quad \forall n = 1, 2, \dots, N, \quad (24b)$$

As it will be shown in the sequel, the form of the objective in (24a) enables us to deal with the non-convex constraint (24b), provided that (24a) can be reformulated into a differentiable function. To this end, a convenient approach is to resort to the Sequential Fractional Programming (SFP) optimization method, also known as majorization-minimization, or inner approximation method [10], [52]–[55].

The basic idea of the SFP method is to tackle a difficult problem by solving a sequence of approximate subproblems. If each approximate problem fulfills some assumptions with respect to the original problem, then the sequence converges and first-order optimality holds upon convergence. In more detail, consider the following general optimization program:

$$\min_{\mathbf{x}} \bar{f}(\mathbf{x}) \quad (25a)$$

$$\text{s.t. } g_i(\mathbf{x}) \leq 0 \quad \forall i = 1, 2, \dots, I. \quad (25b)$$

Consider also the sequence $\{\mathbf{x}^{(t)}\}$ of feasible points for (25), and the sequence of minimization problems $\mathcal{P}_{\mathbf{x}^{(t)}}$ with objectives $f(\mathbf{x}|\mathbf{x}^{(t)})$ and the same constraints as (25). If for each $\mathbf{x}^{(t)}$ the following conditions are fulfilled:

- 1) $f(\mathbf{x}|\mathbf{x}^{(t)}) \geq \bar{f}(\mathbf{x})$ for all feasible \mathbf{x} ,
- 2) $f(\mathbf{x}^{(t)}|\mathbf{x}^{(t)}) = \bar{f}(\mathbf{x}^{(t)})$,
- 3) $\nabla_{\mathbf{x}}f(\mathbf{x}^{(t)}|\mathbf{x}^{(t)}) = \nabla_{\mathbf{x}}\bar{f}(\mathbf{x}^{(t)})$,

then the optimal sequence $\{f(\mathbf{x}^*)^{(t)}\}$ of the optimal values of problems $\mathcal{P}_{\mathbf{x}^{(t)}}$ is monotonically decreasing and converges. Moreover, upon convergence, the first-order optimality properties of problem (25) are satisfied [10], [52]–[55]. Clearly, the usefulness of the SFP method depends on the possibility of determining suitable functions $f(\mathbf{x}|\mathbf{x}^{(t)})$ meeting the above three conditions. In addition, these functions need to be easier than (24a) to minimize.

For the optimization problem (24) at hand, the SFP method can be applied as described in the rest of this section. We commence with the following lemma that provides a convenient upper bound for the objective $\mathbf{y}^H \mathbf{A} \mathbf{y}$ in (24a) (the definition $\mathbf{y} = \text{vec}(\Phi^{-1})$ in (14) is reused).

Lemma 1: For any feasible \mathbf{y} for (24), and given any feasible point $\mathbf{y}^{(t)}$, a suitable upper bound to employ the SFP method is:

$$\mathbf{y}^H \mathbf{A} \mathbf{y} \leq f(\mathbf{y}|\mathbf{y}^{(t)}) = \mathbf{y}^H \mathbf{M} \mathbf{y} - 2\text{Re}(\mathbf{y}^H (\mathbf{M} - \mathbf{A}) \mathbf{y}^{(t)}) + (\mathbf{y}^{(t)})^H (\mathbf{M} - \mathbf{A}) \mathbf{y}^{(t)}, \quad (26)$$

where $\mathbf{M} \triangleq \lambda_{\max} \mathbf{I}_{N^2}$ with λ_{\max} being the maximum eigenvalue of \mathbf{A} .

Proof: Let us consider the following inequality:

$$\|(\mathbf{M} - \mathbf{A})^{1/2} \mathbf{y} - (\mathbf{M} - \mathbf{A})^{1/2} \mathbf{y}^{(t)}\|^2 \geq 0. \quad (27)$$

Since the matrix $\mathbf{M} - \mathbf{A}$ is positive semidefinite by construction, elaborating the latter inequality yields

$$\mathbf{y}^H (\mathbf{M} - \mathbf{A}) \mathbf{y} + (\mathbf{y}^{(t)})^H (\mathbf{M} - \mathbf{A}) \mathbf{y}^{(t)} - 2\text{Re}(\mathbf{y}^H (\mathbf{M} - \mathbf{A}) \mathbf{y}^{(t)}) \geq 0. \quad (28)$$

By isolating the term $\mathbf{y}^H \mathbf{A} \mathbf{x}$, we obtain the bound in (26); this completes the proof. \blacksquare

Lemma 1 provides a suitable expression for the surrogate function in terms of the variable \mathbf{y} to be used with the SFP method. The next step is to reformulate constraint (24b) also in terms of the variable \mathbf{y} . Here, it should be paid attention to the fact that (24b) enforces the diagonal elements of Φ to have unit modulus, whereas \mathbf{y} contains the elements of the vectorized Φ . Thus, only some elements of \mathbf{y} need to have unit modulus, while all others are bound to be zero. More precisely, the \mathbf{y} 's elements that must have unit modulus are those with indices of the form $(i - 1)N + i$, with $i = 1, 2, \dots, N$. For example, if $N = 5$, we have the indices $\{1, N + 2, 2N + 3, 3N + 4, 4N + 5 = N^2 = 25\}$.

Putting all above together, each iteration of the SFP method requires solving the following problem with respect to the variable \mathbf{y} (from which the optimal Φ can be easily obtained):

$$\min_{\mathbf{y}} f(\mathbf{y}|\mathbf{y}^{(t)}) \quad (29a)$$

$$\text{s.t. } |y_i| = 1, \forall i = (n-1)N + n, n = 1, 2, \dots, N, \quad (29b)$$

$$y_i = 0, \forall i \neq (n-1)N + n, n = 1, 2, \dots, N, \quad (29c)$$

where y_n denotes the n -element of vector \mathbf{y} . In the following lemma we present the solution for (29).

Lemma 2: For any $\mathbf{y}^{(t)}$, the optimization problem (29) is solved by

$$y_i = \begin{cases} e^{j\arg(c_i)}, \forall i = (n-1)N + n, n = 1, 2, \dots, N \\ 0, \quad \forall i \neq (n-1)N + n, n = 1, 2, \dots, N \end{cases}, \quad (30)$$

where c_i with $i = 1, 2, \dots, N^2$ is the i -th element of $\mathbf{c} \triangleq (\lambda_{\max}\mathbf{I}_{N^2} - \mathbf{A})\mathbf{y}^{(t)}$.

Proof: The objective function (29a) can be expressed as

$$f(\mathbf{y}|\mathbf{y}^{(t)}) = \lambda_{\max}\|\mathbf{y}\|^2 - 2\text{Re}(\mathbf{y}^H(\lambda_{\max}\mathbf{I}_{N^2} - \mathbf{A})\mathbf{y}^{(t)}) + (\mathbf{y}^{(t)})^H(\lambda_{\max}\mathbf{I}_{N^2} - \mathbf{A})\mathbf{y}^{(t)}. \quad (31)$$

By neglecting the terms that do not depend on \mathbf{y} and observing that by virtue of (29b) and (29c) it holds $\|\mathbf{y}\|^2 = N$, problem (29) can be equivalently recast as

$$\max_{\mathbf{y}} 2\text{Re}(\mathbf{y}^H(\lambda_{\max}\mathbf{I}_{N^2} - \mathbf{A})\mathbf{y}^{(t)}) \quad (32a)$$

$$\text{s.t. } |y_i| = 1, \forall i = (j-1)N + j, j = 1, 2, \dots, N, \quad (32b)$$

$$y_i = 0, \forall i \neq (j-1)N + j, j = 1, 2, \dots, N. \quad (32c)$$

Clearly, the only free variables are the phases of the y_i 's components whose modulus is constrained to be unity, whereas all other components of \mathbf{y} are constrained to be zero. Then, (32a) can be seen to be maximized when the phases of the non-zero components of y_i 's are aligned with those of the corresponding components of the vector $(\lambda_{\max}\mathbf{I}_{N^2} - \mathbf{A})\mathbf{y}^{(t)}$. Hence, (30) is obtained. ■

Algorithm 1 Dinkelbach's Method

- 1: **Initialization:** $K, b, \xi, P_{\text{BS}}, P_{\text{UE}}, P_n(b), \epsilon > 0$, and $\lambda_0 = 0$.
 - 2: **for** $i = 1, 2, \dots$ **do**
 - 3: Solve the concave maximization:

$$\mathbf{P}_i^* = \arg \max_{\mathbf{P} \in \mathcal{B}} \sum_{k=1}^K \log_2(1 + p_k \sigma^{-2}) - \lambda_{i-1} (\xi \sum_{k=1}^K p_k + P_{\text{BS}} + K P_{\text{UE}} + N P_n(b)).$$
 - 4: Set $\lambda_i = \frac{\sum_{k=1}^K \log_2(1 + p_{k,i}^* \sigma^{-2})}{\xi \sum_{k=1}^K p_{k,i}^* + P_{\text{BS}} + K P_{\text{UE}} + N P_n(b)}$.
 - 5: **if** $|\lambda_i - \lambda_{i-1}| < \epsilon$ **then**
 - 6: **Output:** \mathbf{P}_i^* .
 - 7: **end if**
 - 8: **end for**
-

B. Optimization with respect to the Power Allocation \mathbf{P}

We now turn again our attention in problem (8) for the case where Φ is fixed and the objective is the optimization over \mathbf{P} . Particularly, we focus on solving:

$$\max_{\mathbf{P}} \frac{\sum_{k=1}^K \log_2(1 + p_k \sigma^{-2})}{\xi \sum_{k=1}^K p_k + P_{\text{BS}} + K P_{\text{UE}} + N P_n(b)} \quad (33a)$$

$$\text{s.t. } p_k \geq \sigma^2(2^{R_{\min,k}} - 1), \quad \forall k = 1, 2, \dots, K, \quad (33b)$$

$$\text{tr}((\mathbf{H}_2 \Phi \mathbf{H}_1)^+ \mathbf{P} (\mathbf{H}_2 \Phi \mathbf{H}_1)^{+H}) \leq P_{\max}. \quad (33c)$$

It is can be that, for fixed Φ , the numerator of (33a) is concave in \mathbf{P} , while the denominator of (33a) is affine in \mathbf{P} . Moreover, both constraints (33b) and (33c) are also affine with respect to \mathbf{P} . As a consequence, problem (33) is a single-ratio maximization problem that can be globally solved with limited complexity using Dinkelbach's algorithm [10]. This method is summarized in Algorithm 1, where $\mathcal{B} \triangleq \{\mathbf{P} = \text{diag}[p_1, p_2, \dots, p_K] : (33b) \& (33c)\}$ and $\mathbf{P}_i^* \triangleq \text{diag}[p_{1,i}^*, p_{2,i}^*, \dots, p_{K,i}^*]$ denotes the transmit power allocation solution in Step 3 at each i -th (with $i = 1, 2, \dots$) algorithmic iteration.

Putting together the solutions for Φ and \mathbf{P} presented respectively in Sections III-A and III-B, our two proposed EE maximization algorithms for the considered RIS-based multi-user MISO system are summarized in Algorithms 2 and 3. As shown, the solutions for Φ and \mathbf{P} are alternatively and iteratively updated till reaching convergence. Specifically, since at each iteration ℓ , both approaches increase the EE value, i.e. $\text{EE}^{(\ell+1)} \geq \text{EE}^{(\ell)}$ for all ℓ , convergence of the algorithm in the value of the objective is guaranteed. Indeed, the objective is upper-bounded

over the feasible set of (8), and thus can not increase indefinitely [50], [51], [56]–[61]. However, no global optimality claim can be made due to the following facts: *i*) problem (8) is not jointly convex with respect to both \mathbf{P} and Φ ; and *ii*) the proposed methods for optimizing Φ (when \mathbf{P} is fixed) are not guaranteed to yield the globally optimal phase matrix.

C. Sum Rate Maximization

In the previous sections we focused on the EE maximization problem (8). It should be stressed, however, that sum-rate maximization is a special case of the considered EE maximization problem. More specifically, it can be seen from (8) that the system sum rate performance is given by the numerator in (8a). Hence, Algorithm 2 can be specialized to perform sum rate maximization by simply setting $\xi = 0$, since in this case the denominator of (8a) reduces to a constant. In particular, this modification affects the optimization with respect to the transmit powers, which reduces to a non-fractional and convex problem that can be solved by a single iteration of Algorithm 1.

D. Computational Complexity

The computational complexity of the proposed algorithms depends on the number of iterations of the alternating maximization, say I_{alt} , and on the complexity required to solve each sub-problem.

As for Algorithm 2, it can be seen that the optimization of the RIS phase shifts depends on the number of gradient updates, say I_{gd} , times the amount of operations performed in each gradient update, which can be seen to scale with⁴ N^2 complex multiplications. On the other hand, the optimization of the transmit powers requires to perform I_D Dinkelbach's iterations, each requiring to solve a convex problem. Thus, recalling that convex problems have a polynomial complexity in the number of optimization variables, which is at most quartic in the number of variables [62], the asymptotic complexity of Algorithm 2 can be evaluated as

$$\mathcal{O}(I_{alt}(I_{gd}N^2 + I_D K^p)), \quad (34)$$

with $1 \leq p \leq 4$. As for the values of I_{alt} , I_{gd} , and I_D , deriving closed-form expressions as a function of the system parameters appears prohibitive. Nevertheless, our numerical results

⁴The complexity of additions is negligible compared to that required for the multiplications.

Algorithm 2 Gradient-based EE Maximization Algorithm

- 1: **Input:** $K, b, \xi, P_{BS}, P_{UE}, P_n(b), P_{\max}, \sigma^2, \{R_{\min,k}\}_{k=1}^K, \mathbf{H}_2, \mathbf{H}_1,$ and $\epsilon > 0.$
 - 2: **Initialization:** $\mathbf{P}^0 = \frac{P_{\max}}{K} \mathbf{I}_K, \Phi^0 = \frac{\pi}{2} \mathbf{I}_N, \mathbf{q}^0 = \nabla_{\Theta}((\mathbf{y}^0)^H \mathbf{A} \mathbf{y}^0),$ and $\mathbf{d}^0 = -\mathbf{q}^0.$
 - 3: **while** $|\text{EE}^{(\ell+1)} - \text{EE}^{(\ell)}|^2 > \epsilon,$ **do**
 - 4: Given \mathbf{P} update Φ :
 - 5: **for** $t = 0, 1, 2, \dots$ **do**
 - 6: $\mathbf{y}_1^{(t)} = \mathbf{y}^{(t)} \circ \mathbf{d}^{(t)}.$
 - 7: $\mathbf{y}_2^{(t)} = \mathbf{y}^{(t)} \circ \mathbf{d}^{(t)} \circ \mathbf{d}^{(t)}.$
 - 8: $z_2 = \text{Im}((\mathbf{y}^{(t)})^H \mathbf{A} \mathbf{y}_1^{(t)}),$
 - 9: $z_3 = \text{Re}((\mathbf{y}^{(t)})^H \mathbf{A} \mathbf{y}_2^{(t)}) - (\mathbf{y}_1^{(t)})^H \mathbf{A} \mathbf{y}_1^{(t)}.$
 - 10: Compute $\hat{h}(\mu) = 0$ using (22).
 - 11: Set the step size as $\mu = -\frac{z_2}{z_3}.$
 - 12: $\mathbf{y}^{(t+1)} = \mathbf{y}^{(t)} \circ e^{j\mu \mathbf{d}^{(t)}} \circ \text{vec}(\mathbf{I}_N).$
 - 13: $\mathbf{q}^{(t+1)} = 2\text{Re}(-j(\mathbf{y}^*)^{(t+1)} \circ (\mathbf{A} \mathbf{y}^{(t+1)})).$
 - 14: $\mathbf{d}^{(t+1)} = -\mathbf{q}^{(t+1)} + \frac{(\mathbf{q}^{(t+1)} - \mathbf{q}^{(t)})^T \mathbf{q}^{(t+1)}}{\|\mathbf{q}^{(t)}\|^2} \mathbf{d}^{(t)}.$
 - 15:
$$\mathbf{d}^{(t+1)} = \begin{cases} \mathbf{d}^{(t+1)}, & (\mathbf{q}^{(t+1)})^T \mathbf{d}^{(t+1)} < 0 \\ -\mathbf{q}^{(t+1)}, & (\mathbf{q}^{(t+1)})^T \mathbf{d}^{(t+1)} \geq 0 \end{cases}.$$
 - 16: **Until** $\|\Phi^{(t+1)} - \Phi^{(t)}\|^2 < \epsilon;$ Obtain $\Phi^{(\ell+1)} = \Phi^{(t+1)}.$
 - 17: **end for**
 - Given Φ update \mathbf{P} :
 - 18: **if** (10a) evaluated at $\Phi^{(\ell+1)}$ is lower than P_{\max} **then:**
 - 19: Update \mathbf{P} by solving the following problem using Algorithm 1:
 - 20:
$$\mathbf{P}^{(\ell+1)} = \arg \max_{\mathbf{P} \in \mathcal{B}} \frac{\sum_{k=1}^K \log_2(1 + p_k \sigma^{-2})}{\xi \sum_{k=1}^K p_k + P_{BS} + K P_{UE} + N P_n(b)}$$
 - 21: **elseBreak** and declare infeasibility.
 - 22: **end if**
 - 23: **end while**
 - 24: **Output:** Φ and $\mathbf{P}.$
-

confirm that convergence occurs in a few iterations. Moreover, as for I_D , it is known that Dinkelbach's algorithm exhibits a super-linear convergence rate [10].

A similar analysis holds for Algorithm 3, with the only difference that the complexity of

Algorithm 3 Sequential programming EE Maximization Algorithm

- 1: **Input:** $K, b, \xi, P_{BS}, P_{UE}, P_n(b), P_{\max}, \sigma^2, \{R_{\min,k}\}_{k=1}^K, \mathbf{H}_2, \mathbf{H}_1,$ and $\epsilon > 0.$
- 2: **Initialization:** $\mathbf{P}^0 = \frac{P_{\max}}{K} \mathbf{I}_K$ and $\Phi^0 = \frac{\pi}{2} \mathbf{I}_N.$
- 3: **while** $|\text{EE}^{(\ell+1)} - \text{EE}^{(\ell)}|^2 > \epsilon,$ **do**
 Optimize with respect to Φ given \mathbf{P} :
 - 4: **for** $t = 0, 1, 2, \dots$ **do**
 - 5: $\mathbf{A} = (\overline{\mathbf{H}}_2^{+H} \otimes \mathbf{H}_1^+)^H (\overline{\mathbf{H}}_2^{+H} \otimes \mathbf{H}_1^+).$
 - 6: $\mathbf{y} \triangleq \text{vec}(\Phi^{-1}).$
 - 7: Compute \mathbf{y} as in (30).
 - 8: $\mathbf{y}^{(t+1)} = \text{reshape}(\mathbf{y});$
 - 9: **Until** $\|\Phi^{(t+1)} - \Phi^{(t)}\|^2 < \epsilon,$
 - 10: Obtain $\Phi^{(\ell+1)} = \Phi^{(t+1)};$
 - 11: **end for**
 Optimize with respect to \mathbf{P} given Φ :
 - 12: **if** (10a) evaluated at $\Phi^{(\ell+1)}$ is lower than P_{\max} **then:**
 - 13: Update \mathbf{P} by solving the following problem using Algorithm 1:
 - 14:
$$\mathbf{P}^{(\ell+1)} = \arg \max_{\mathbf{P} \in \mathcal{B}} \frac{\sum_{k=1}^K \log_2(1+p_k \sigma^{-2})}{\xi \sum_{k=1}^K p_k + P_{BS} + K P_{UE} + N P_n(b)}$$
 - 15: **else** Break and declare infeasibility.
 - 16: **end if**
 - 17: **end while**
 - 18: **Output:** $\Phi^{(\ell+1)}$ and $\mathbf{P}^{(\ell+1)}.$

optimizing the RIS phase shifts is given by $I_{seq} N^q$, with $1 \leq q \leq 4$, since phase optimization performs I_{seq} iterations of the sequential optimization method, each requiring the solution of a convex problem with N variables. Thus, the asymptotic complexity of Algorithm 3 can be evaluated as

$$\mathcal{O}(I_{alt}(I_{seq} N^q + I_D K^p)). \quad (35)$$

IV. NUMERICAL RESULTS

In this section, we investigate the performance of the RIS-based K -user MISO communication system illustrated in Fig. 2. The multiple single-antenna mobile users are assumed randomly and uniformly placed in the $100m \times 100m$ half right-hand side rectangular of the figure. All

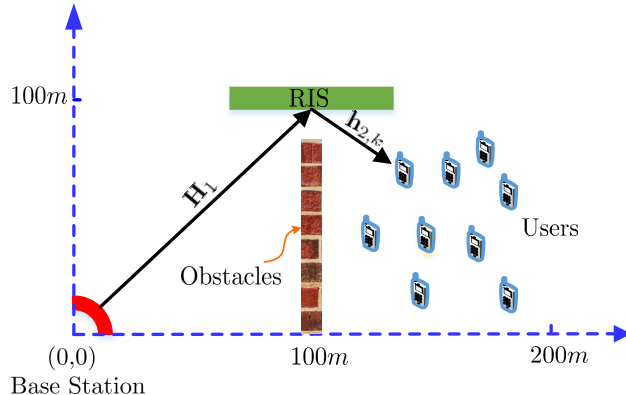


Figure 2. The simulated RIS-based K -user MISO communication scenario comprising of a M -antenna base station and a N -element intelligent surface.

Table I
SIMULATION AND ALGORITHMIC PARAMETERS

Parameters	Values
RIS central element placement:	$(100m, 100m)$
BS central element placement:	$(0, 0)$
Small scale fading model $\forall i, k, j$:	$[\mathbf{H}_1]_{ij}, [\mathbf{h}_{2,k}]_i \sim \mathcal{CN}(0, 1)$
Large scale fading model at distance d :	$\frac{10^{-3.53}}{d^{3.76}}$
Transmission bandwidth BW:	180kHz
Circuit dissipated power at BS P_{BS} :	9dBW
Circuit dissipated power coefficients at BS ξ and AF relay ξ_{AF} :	1.2
Maximum transmit power at BS and AF relay $P_{\max}=P_{R,\max}$:	20dBW
Dissipated power at each user P_{UE} :	10dBm
Dissipated power at the n -th RIS element $P_n(b)$:	10dBm
Dissipated power at each AF relay transmit-receive antenna P_R :	10dBm
Algorithmic convergence parameter:	$\epsilon = 10^{-3}$

presented illustrations have been averaged results over 10^3 independent realizations of the users' positions and channel realizations, generated according to the 3GPP propagation environment described in [63], whose parameters are summarized in Table I. Therein, $[\mathbf{H}_1]_{ij}$ and $[\mathbf{h}_{2,k}]_i$ with $i = 1, 2, \dots, N$, $k = 1, 2, \dots, K$, and $j = 1, 2, \dots, M$ denote the (i, j) -th and i -th elements of the respective matrices. In the table above, we also include the hardware dissipation parameters of [10], [13] for BS, RIS, and the mobile users, as well as for the AF relay that will be used for performance comparisons purposes. The relay is assumed to transmit with maximum power $P_{R,\max}$, which is considered in all performance results equal to P_{\max} .

Without loss of generality, in the figures that follow we assume equal individual rate constraints for all K users, i.e., $R_{\min,k} = R_{\min} \forall k$. In addition, we set R_{\min} to a fraction of the rate that each user would have in the genie case of mutually orthogonal channels and uniform power allocation. In particular, this genie rate for each k -th mobile user is given by

$$R = \log_2 \left(1 + \frac{P_{\max}}{K\sigma^2} \right). \quad (36)$$

Thus, the QoS constraints depend on P_{\max} , which ensures that the minimum rate is commensurate to the maximum power that can be used, in turn leading to a feasibility rate of Problem (8) that is approximately constant with P_{\max} . Table II below shows the feasibility rate obtained for $P_{\max} = 20$ dBW and different fractions R .

Table II
DIFFERENT QOSS VS FEASIBILITY RATE

QoS (bps/Hz)	0.1R	0.2R	0.3R	0.4R	0.5R
Feasibility Rate (%)	99.44	99.44	99.44	99.23	99.02

Moreover, we mention that, in the very few unfeasible scenarios encountered in our simulation, we have relaxed the QoS constraint and deployed the corresponding solution. In light of the high feasibility rate shown above, this has a negligible impact on the shown results.

A. Benchmark: Amplify-and-Forward Relay

It is reasonable to expect that the consideration of a reconfigurable RIS structure in the investigated scenario of Fig. 2 provides substantial EE gains compared to the case where such a surface is absent; this intuition has been verified via simulations in [1]. Hereinafter, we consider a more relevant to Fig. 2 benchmark scheme that includes a conventional N -antenna AF relay [32]–[35] in the place of the RIS structure. To ensure a fair comparison between this benchmark scheme and our proposed RIS-based one in the performance results that follow, we have considered the same users' positions and channel realizations in both cases. Similar to the RIS case modeled by the phase shifting matrix Φ , we assume that the relay deploys the $N \times N$ complex diagonal AF matrix \mathbf{V} . Differently from Φ , \mathbf{V} 's diagonal elements are not constrained to have unit modulus, but rather a maximum relay power constraint is enforced. In more detail,

the baseband received signals $\mathbf{y}_R \in \mathbb{C}^{N \times 1}$ and $\mathbf{y}_K \in \mathbb{C}^{K \times 1}$ at the relay and at all K mobile users, respectively, can be expressed as

$$\mathbf{y}_R \triangleq \mathbf{H}_1 \mathbf{x} + \mathbf{w}_R, \quad (37)$$

$$\mathbf{y}_K \triangleq \mathbf{H}_2 \mathbf{V} \mathbf{y}_R + \mathbf{w}_K = \mathbf{H}_2 \mathbf{V} \mathbf{H}_1 \mathbf{x} + \mathbf{H}_2 \mathbf{V} \mathbf{w}_R + \mathbf{w}_K, \quad (38)$$

where $\mathbf{w}_R \in \mathbb{C}^{N \times 1}$ denote the thermal noise at relay modeled as a zero-mean complex circularly Gaussian vector with covariance matrix \mathbf{I}_N . We model similarly the thermal noises at all K users, which are included in $\mathbf{w}_K \in \mathbb{C}^{K \times 1}$ having covariance matrix \mathbf{I}_K .

It is interesting to observe that, since the AF matrix \mathbf{V} is not unitary, it introduces a noise amplification effect that is not present in the RIS case. Moreover, as already anticipated, unlike RIS, the AF relay consumes RF power to amplify the incoming signal. Accounting for ZF transmission from BS as in the RIS design case in (8), the relay power consumption is given by

$$P_{AF} \triangleq \text{tr}(\mathbf{H}_2^+ \mathbf{P} \mathbf{H}_2^{+H} + \mathbf{V} \mathbf{V}^H \sigma^2). \quad (39)$$

Hence, for the case of AF relaying, we consider the following EE maximization problem for the joint design of \mathbf{P} and \mathbf{V} :

$$\max_{\mathbf{V}, \mathbf{P}} \frac{\sum_{k=1}^K \log_2 \left(1 + \frac{p_k}{|\mathbf{h}_{2,k} \mathbf{V} \mathbf{V}^H \mathbf{h}_{2,k}^H|^2 + \sigma^2} \right)}{\xi \sum_{k=1}^K p_k + P_{BS} + K P_{UE} + \xi_{AF} P_{AF} + N P_R} \quad (40a)$$

$$\text{s.t. } \log_2 \left(1 + \frac{p_k}{|\mathbf{h}_{2,k} \mathbf{V} \mathbf{V}^H \mathbf{h}_{2,k}^H|^2 + \sigma^2} \right) \geq R_{\min,k} \quad \forall k = 1, 2, \dots, K, \quad (40b)$$

$$\text{tr}((\mathbf{H}_2 \mathbf{V} \mathbf{H}_1)^+ \mathbf{P} (\mathbf{H}_2 \mathbf{V} \mathbf{H}_1)^{+H}) \leq P_{\max}, \quad (40c)$$

$$\text{tr}(\mathbf{H}_2^+ \mathbf{P} \mathbf{H}_2^{+H} + \mathbf{V} \mathbf{V}^H \sigma^2) \leq P_{R,\max}, \quad (40d)$$

where ξ_{AF} depends on the efficiency of the relay power amplifier. In order to solve (40) we resort again to the alternating optimization method, like in the RIS case. Moreover, it is assumed that the end-to-end data transmission phase of the relay has the same duration as the end-to-end data transmission duration of the RIS-based system. Hence, no pre-log factor is considered in (40), in analogy with Problem (8).

The optimization with respect to \mathbf{P} for a given \mathbf{V} can be performed following a similar approach to Section III-B, whereas the optimization with respect to \mathbf{V} for a given \mathbf{P} becomes more challenging due to the presence of constraint (40c). To find the optimum \mathbf{V} in the results that follow we have employed numerical exhaustive search.

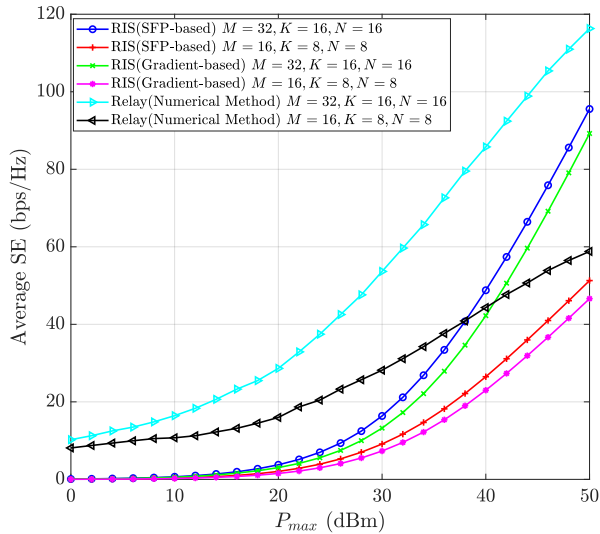


Figure 3. Average SE using either RIS or AF relay versus P_{\max} for $R_{\min} = 0\text{bps/Hz}$ and: a) $M = 32, K = 16, N = 16$; and b) $M = 16, K = 8, N = 8$.

B. RIS vs AF relay Performance Comparison

The achievable SE and EE performances as functions of P_{\max} in dBm are illustrated in Figs. 3 and 4, respectively. We have evaluated the gradient- and SFP-based approaches described in Algorithms 2 and 3, respectively, as well as the algorithm described in Section IV-A for the AF relay case. In both figures, we have set the minimum QoS constraint as $R_{\min} = 0\text{bps/Hz}$ for all K users, and considered the two different settings: a) $M = 32, K = 16$, and $N = 16$; and b) $M = 16, K = 8$, and $N = 8$. As seen from Fig. 3, the relay-assisted system outperforms the RIS-based one, irrespective of the proposed algorithm used. This behavior is expected since the AF relay is an active terminal rather than a reflecting structure as the RIS is. The relay possesses dedicated transmit circuitry that provides the transmit power $P_{R,\max}$ to it. Moreover, the relay is not constrained by the unit modulus constraint that the intelligent surface has. Specifically, RIS loses about 40bps/Hz and 20bps/Hz at $P_{\max} = 30\text{dBm}$ under the settings a) and b), respectively. However, as P_{\max} increases, the performance gap between the RIS and relay cases becomes smaller. This happens because as P_{\max} increases, the relay transmit power $P_{R,\max}$ becomes less and less relevant to the SE, which is actually impacted by the BS transmit power. It can be also observed from Fig. 3, which also holds in Figs. 4, that both proposed Algorithms 2 and 3 perform similarly, with the SFP-based one achieving slightly better performance.

The trend in Fig. 3 is reversed in Fig. 4, where the EE performance is sketched. It is shown that both proposed algorithms for the RIS-based system case significantly outperform our derived

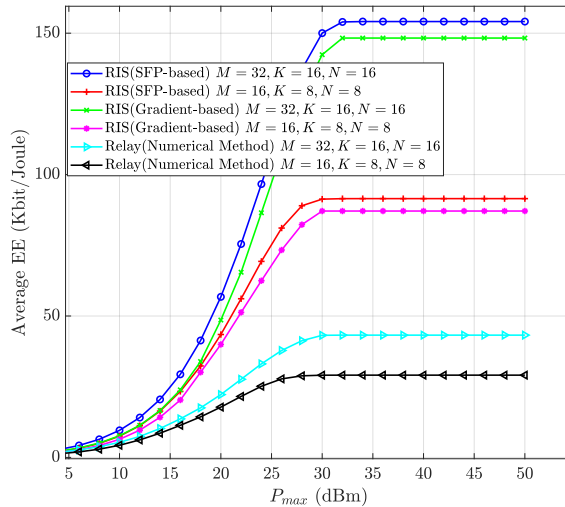


Figure 4. Average EE using either RIS or AF relay versus P_{\max} for $R_{\min} = 0\text{bps/Hz}$ and: a) $M = 32, K = 16, N = 16$; and b) $M = 16, K = 8, N = 8$.

algorithm for the relay-assisted one. Particularly, the EE of the RIS-based system is 300% larger than that of the one based on the AF relay when $P_{\max} \geq 32\text{dBm}$. This is a direct consequence of the fact that former system exhibits a much lower energy consumption compared to the latter one. It is also shown that the setting a) with $M = 32, K = 16$, and $N = 16$ is more energy efficient than the setting b) with $M = 16, K = 8, N = 8$. It can be also observed that for both systems cases the EE performance saturates for $P_{\max} \geq 32\text{dBm}$. This explained by the fact that the EE function is not monotonically increasing with the maximum BS transmit power P_{\max} , but instead has a finite maximizer. When $P_{\max} \geq 32\text{dBm}$, the excess BS transmit power is actually not used since as it would only reduce the EE value.

C. Impact of the QoS Constraints

The effect of the different values for R_{\min} in the SE and EE performances versus P_{\max} in dBm is depicted in Figs. 5 and 6, respectively, using our SFP-based algorithm 3. For the cases where the design problems turned out to be infeasible, the rate constraint has been removed and the unconstrained solutions were retained. Fig. 5 shows that for low P_{\max} values the problem is nearly always infeasible. This is expected since there is not enough transmit power from BS to meet the rate requests of the users, and thus, the performance of all designed solutions coincide to very low SE values. However, for $P_{\max} \geq 16\text{dBm}$, the values for R_{\min} start having a significant impact on the SE. It can be observed that, increasing R_{\min} results in increasing the achievable

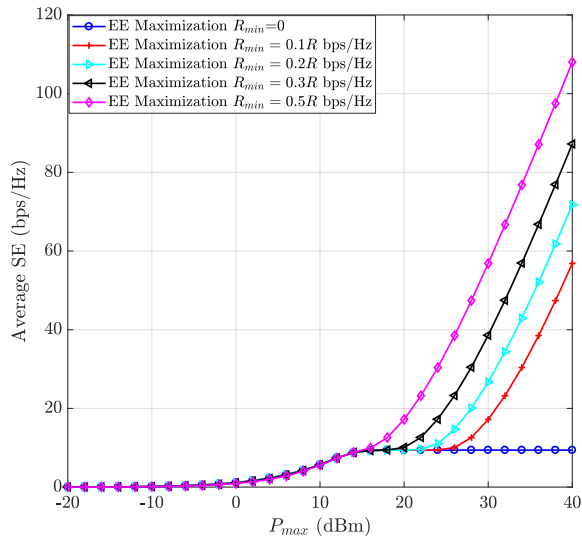


Figure 5. Average SE using RIS versus P_{\max} for $M = 32$, $K = 16$, $N = 16$, as well as different fractions of R for R_{\min} .

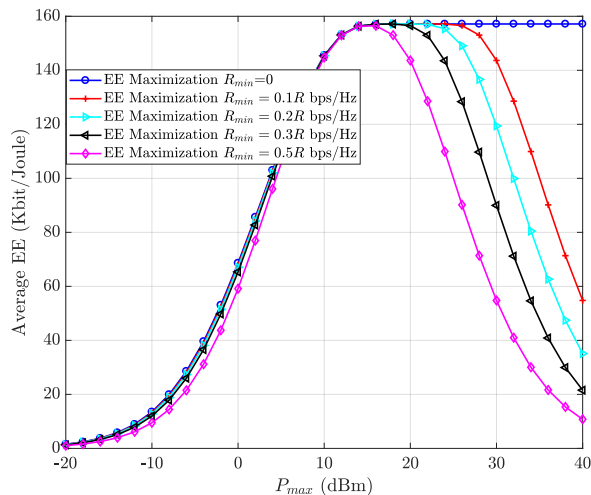


Figure 6. Average EE using RIS versus P_{\max} for $M = 32$, $K = 16$, $N = 16$, as well as different fractions of R for R_{\min} .

SE and outperforming more the saturating unconstrained case of $R_{\min} = 0$ bps/Hz. Obviously, the larger the R_{\min} value is, the higher the slope of the SE curve. The performance behavior in Fig. 6 follows the same trend with Fig. 5. We may see that for larger P_{\max} , enforcing stricter QoS constraints causes the EE to decrease faster, due to the fact that the excess BS transmit power is used to meet the common user rate requirements.

D. Comparison between the SE and EE Maximizing Designs

In Figs. 7 and 8 we plot the average achievable SE and EE performances versus P_{\max} in dBm for the following design objectives: *i*) EE maximization with $R_{\min} = 0$ bps/Hz using Algorithm 2;

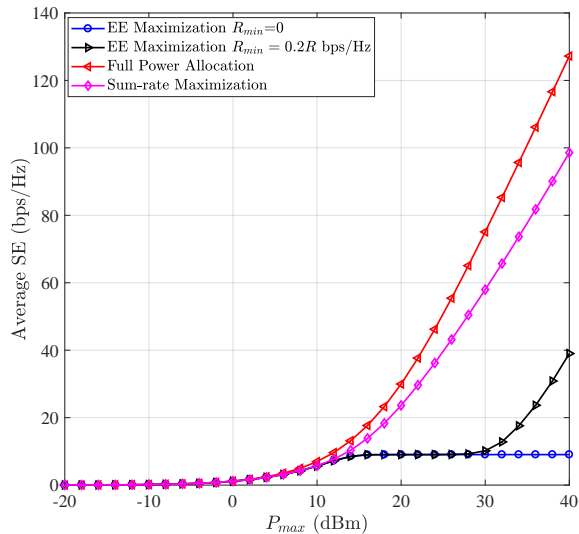


Figure 7. Average SE using RIS versus P_{\max} for $M = 32$, $K = 16$, and $N = 16$ using: a) our SFP-based EE maximization algorithm for $R_{\min} = \{0, 0.2R\}$; b) full power allocation; and c) our SE maximization algorithm.

ii) the same objective and algorithm with *i)* but with $R_{\min} = 0.2R$ bps/Hz; *iii)* SE maximization using the algorithm described in Section III-C; and *iv)* maximum power allocation P_{\max} to each user. It can be seen from both figures that all designs perform similarly for $P_{\max} \leq 15$ dBm, which indicates that the EE and SE objectives are nearly equivalent for such transmit power levels. This can be explained by observing that for low P_{\max} , the EE is an increasing function of the BS transmit power, just as the SE is. In other terms, using full BS transmit power for low P_{\max} is optimal, and in this case, EE maximization reduces to SE maximization. However, as shown for $P_{\max} > 15$ dBm, the EE maximizing objective and the SE one result in designs yielding substantially different performances. For such P_{\max} values, maximizing the SE requires utilizing all available BS power, whereas maximizing EE does require increasing the BS transmit power above a threshold value. As a result, the SE maximization design naturally increases the SE, but leads to decreasing EE. On the contrary, when maximizing EE both the achievable EE and SE performances become constant. It can be also observed from the results of Figs. 8 and 7 that, when EE is maximized subject to QoS constraints, an intermediate behavior is obtained due to the fact that some of the excess transmit power is used in order to fulfill the those constraints. Once the constraints are met, no further BS transmit power is needed.

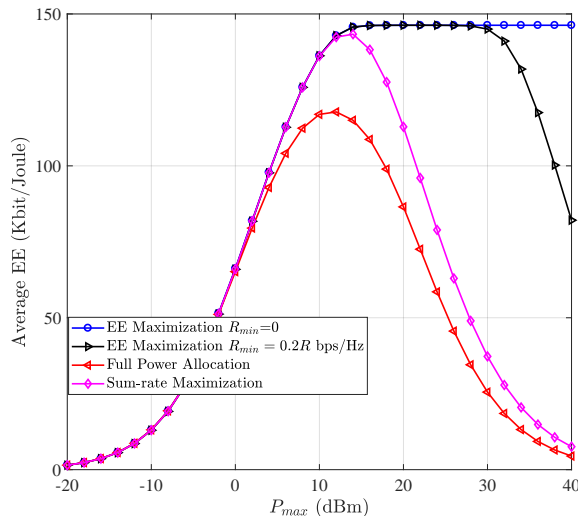


Figure 8. Average EE using RIS versus P_{\max} for $M = 32$, $K = 16$, and $N = 16$ using: a) our SFP-based EE maximization algorithm for $R_{\min} = \{0, 0.2R\}$; b) full power allocation; and c) our SE maximization algorithm.

E. Impact of the number of RIS Elements

In Fig. 9 we consider the gradient- and SFP-based Algorithms for SE maximization, that is a special case of Algorithms 2 and 3 respectively, as described in Section (III-C). The SE performance versus the number of the RIS reflecting elements N is shown. We have set the transmit Signal Noise Ratio (SNR), defined as $\text{SNR} = P_{\max}/\sigma^2$, to 20dB. Other parameters are set as $M = 64$, $K = 64$, and $R_{\min} = 2\text{bps/Hz}$. In this figure, we also report the performance of the optimum SE design obtained by means of numerical global optimization implemented by a numerical grid search. Clearly, this entails an exponential complexity and is considered here only for benchmarking purposes. As clearly shown, both proposed algorithms yield very similar performance curves that are quite close to the ones obtained from the global optimization method. Furthermore, as expected, the larger the N value is, the larger is the achievable SE for the considered RIS-based system.

We finally plot the achieved EE by using the grid search method in Fig.10 versus N . In this figure we consider the following cases for the number of users K , the number of BS antenna elements M , and the power consumption of each RIS b -bit phase resolution element: i) $P_n(b) = 0.01\text{dBm}$, $K = 8$, and $M = 6$; ii) $P_n(b) = 5\text{dBm}$, $K = 8$, and $M = 6$; iii) $P_n(b) = 5\text{dBm}$, $K = 16$, and $M = 12$; and iv) $P_n(b) = 100\text{dBm}$, $K = 8$, and $M = 6$. As observed, when N is quite small, i.e., $N \leq 5$, all designs exhibit the same trend. Particularly,

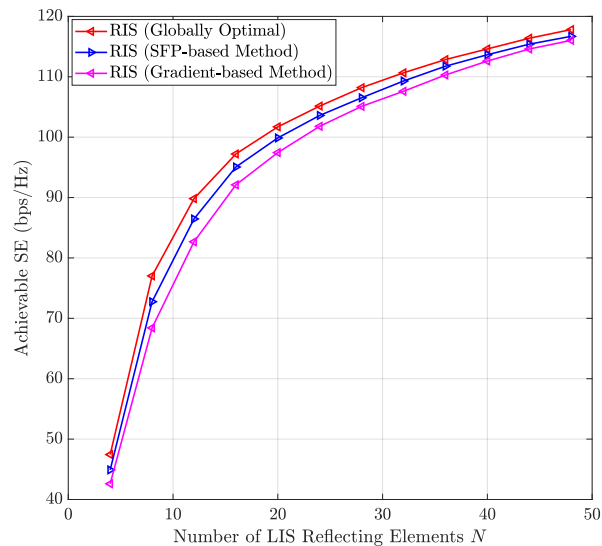


Figure 9. Average SE using RIS versus N for $\text{SNR} = 20\text{dB}$, $M = 64$, $K = 64$ and $R_{\min} = 2\text{bps/Hz}$ with both our presented algorithms as well as exhaustive global optimization.

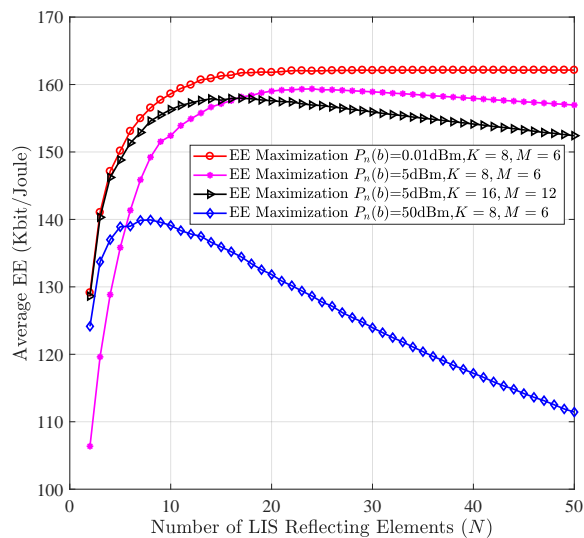


Figure 10. Average EE using RIS versus N for $\text{SNR} = -10\text{dB}$ and $R_{\min} = 0\text{bps/Hz}$, as well as: a) $P_n(b) = 0.01\text{dBm}$, $K = 8$, and $M = 6$; b) $P_n(b) = 5\text{dBm}$, $K = 8$, and $M = 6$; c) $P_n(b) = 5\text{dBm}$, $K = 16$, and $M = 12$; and d) $P_n(b) = 100\text{dBm}$, $K = 8$, and $M = 6$. Note that the EE performance is implemented by a grid search method.

EE performance increases as N increases. However, for a small-to-moderate N value and on, EE starts decreasing. This behavior seems not to happen for $P_n(b) = 0.01\text{dBm}$, but this is only due to the fact that this value of $P_n(b)$ is quite small, and thus it would take a very large N to observe EE decreasing. The results in Fig.10 confirm that there exists an optimal number N of RIS elements as far as the EE maximization objective is concerned. In other words, an optimal trade-off exists between the rate benefit of deploying larger and larger RIS structure and its corresponding energy consumption cost.

V. CONCLUSION AND FUTURE WORK

In this paper, we considered a RIS-based downlink multi-user MISO system and presented two computationally efficient EE maximization algorithms for the BS transmit power allocation and the RIS reflector values. Both algorithms were based on alternating maximization, with the one adopting gradient descent for the RIS design, while the other is a SFP-based approach. The optimal transmit power allocation was tackled by a fractional programming method. Special cases of both algorithms were used for the SE maximization design. Our numerical results showed that the proposed SFP-based approach achieves near optimal SE performance, and that RIS-based communication can provide up to 300% higher EE than the relay-assisted one. It was also substantiated that the EE-optimal operating point depends on the numbers of mobile users and RIS elements, as well as the individual power consumption of the RIS elements.

This paper has provided a first contribution in the area of radio resource allocation in cellular communication systems incorporating RIS structures. Many relevant extensions of work can be identified. First of all, this work has considered intelligent surfaces with discrete units, while the investigation of RIS with reflecting elements coated on the surface in continuity appears as a relevant future research direction. In this context, it becomes relevant to analyze the asymptotic regime in which the number of RIS elements tends to infinity, as well as the study of how EE varies with the area of the surface. Other interesting research directions include the consideration of the direct channel between the BS and the mobile users, the acquisition of channel knowledge when a RIS is included, as well as a thorough study of the trade-off between EE and SE in RIS-assisted communication systems. The impact of channel estimation and feedback overhead on the performance of RIS-based systems needs to be analyzed in detail, too. Finally, another future interesting line of research is the investigation of the impact of the area of RIS on the performance. In [14], [64] it was shown that dividing a given surface area into multiple, smaller,

RIS provides more robustness, at the cost of higher feedback and complexity overheads. The optimal trade-off in this context needs to be determined.

ACKNOWLEDGEMENT

The work of C. Yuen was supported by the MIT-SUTD International design center and NSFC 61750110529 Grant, and that of C. Huang by the PHC Merlion PhD program. The work of A. Zappone and M. Debbah was supported by H2020 MSCA IF BESMART, Grant 749336. The work of M. Debbah was also supported by the H2020-ERC PoC-CacheMire, Grant 727682.

REFERENCES

- [1] C. Huang et al., "Achievable rate maximization by passive intelligent mirrors," in *Proc. IEEE ICASSP*, Calgary, Canada, Apr. 2018, pp. 1–6.
- [2] "NGMN alliance 5G white paper," [Online] <https://www.ngmn.org/5g-white-paper/5g-white-paper.html>, 2015.
- [3] Q. Wu et al., "An overview of sustainable green 5G networks," *IEEE Wireless Commun. Mag.*, vol. 24, no. 4, pp. 72–80, Aug 2017.
- [4] Ericsson White Paper, "More than 50 billion connected devices," Tech. Rep. 284 23-3149 Uen, Ericsson, Feb. 2011.
- [5] T. S. Rappaport et al., "Millimeter wave mobile communications for 5G cellular: It will work!," *IEEE Access*, vol. 1, pp. 335–349, 2013.
- [6] G. C. Alexandropoulos et al., "Advanced coordinated beamforming for the downlink of future LTE cellular networks," *IEEE Commun. Mag.*, vol. 54, no. 7, pp. 54–60, Jul. 2016.
- [7] J. Zuo et al., "Energy-efficient downlink transmission for multicell massive das with pilot contamination," *IEEE Trans. on Veh. Tech.*, vol. 66, no. 2, pp. 1209–1221, Feb 2017.
- [8] R. Mahapatra et al., "Energy efficiency tradeoff mechanism towards wireless green communication: A survey," *IEEE Commun. Surveys Tutorials*, vol. 18, no. 1, pp. 686–705, First quarter 2016.
- [9] S. Buzzi et al., "A survey of energy-efficient techniques for 5G networks and challenges ahead," *IEEE J. Sel. Areas Commun.*, vol. 34, no. 4, pp. 697–709, Apr. 2016.
- [10] A. Zappone and E. A. Jorswieck, "Energy efficiency in wireless networks via fractional programming theory," *Found. Trends in Commun. Inf. Theory*, vol. 11, no. 3–4, pp. 185–396, 2015.
- [11] F. Rusek et al., "Scaling up MIMO: Opportunities and challenges with very large arrays," *IEEE Signal Process. Mag.*, vol. 30, no. 1, pp. 40–60, Jan. 2013.
- [12] X. Gao et al., "Massive MIMO in real propagation environments: Do all antennas contribute equally?," *IEEE Trans. Commun.*, vol. 63, no. 11, pp. 3917–3928, Nov. 2015.
- [13] E. Björnson et al., "Massive MIMO systems with non-ideal hardware: Energy efficiency, estimation, and capacity limits," *IEEE Trans. Inf. Theory*, vol. 60, no. 11, pp. 7112–7139, Nov. 2014.
- [14] S. Hu et al., "Beyond massive MIMO: The potential of data transmission with large intelligent surfaces," *IEEE Trans. Signal Process.*, vol. 66, no. 10, pp. 2746–2758, May 2018.
- [15] S. V. Hum and J. Perruisseau-Carrier, "Reconfigurable reflectarrays and array lenses for dynamic antenna beam control: A review," *IEEE Trans. Antennas Prop.*, vol. 62, no. 1, pp. 183–198, Jan. 2014.

- [16] G. C. Alexandropoulos et al., "Precoding for multiuser MIMO systems with single-fed parasitic antenna arrays," in *Proc. IEEE GLOBECOM*, Austin, USA, Dec. 2014, pp. 3656–3661.
- [17] M. A. Sedaghat et al., "A novel single-RF transmitter for massive MIMO," in *Proc. WSA*, Erlangen, Germany, Mar. 2014, pp. 1–8.
- [18] C. Huang et al., "Energy efficient multi-user MISO communication using low resolution large intelligent surfaces," in *IEEE GLOBECOM Workshops*, Abu Dhabi, UAE, Dec. 2018, pp. 1–6.
- [19] S. Hu et al., "User assignment with distributed large intelligent surface (LIS) systems," in *IEEE WCNC*, Barcelona, Spain, Apr. 2018.
- [20] Q. Wu et al., "Intelligent reflecting surface enhanced wireless network: Joint active and passive beamforming design," [Online] <http://arxiv.org/abs/1809.01423>, 2018.
- [21] C. Liaskos et al., "Using any surface to realize a new paradigm for wireless communications," [Online] <http://arxiv.org/abs/1806.04585>, 2018.
- [22] L. Li et al., "Electromagnetic reprogrammable coding metasurface holograms," *Nat. Commun.*, vol. 8, pp. 1–7, Aug. 2017.
- [23] L. Zhang et al., "Space-time-coding digital metasurfaces," *Nat. Commun.*, vol. 9, pp. 1–11, Oct. 2018.
- [24] H. T. Chen, A. J. Taylor, and N. Yu, "A review of metasurfaces: Physics and applications," *Rep. Prog. Phys.*, vol. 79, no. 7, 2016.
- [25] C. Liaskos, S. Nie, A. I. Tsioliaridou, A. Pitsillides, S. Ioannidis, and I. Akyildiz, "A new wireless communication paradigm through software-controlled metasurfaces," *IEEE Commun. Mag.*, vol. 56, no. 9, pp. 162–169, 2018.
- [26] X. Tan et al., "Increasing indoor spectrum sharing capacity using smart reflect-array," in *Proc. IEEE ICC*, Kuala Lumpur, Malaysia, May 2016, pp. 1–6.
- [27] X. Tan et al., "Enabling indoor mobile millimeter-wave networks based on smart reflect-arrays," in *Proc. IEEE INFOCOM*, Honolulu, USA, Apr. 2018, pp. 1–9.
- [28] S. Foo, "Liquid-crystal reconfigurable metasurface reflectors," in *Proc. IEEE ISAP*, San Diego, USA, Jul. 2017, pp. 2069–2070.
- [29] S. Hu et al., "Capacity degradation with modeling hardware impairment in large intelligent surface," in *IEEE GLOBECOM*, Abu Dhabi, UAE, Dec. 2018, pp. 1–6.
- [30] H. Yang et al., "A programmable metasurface with dynamic polarization, scattering and focusing control," *Sci. Rep.* 6, pp. 1–11, Article No 35692, 2016.
- [31] R. W. Heath, Jr. et al., "A current perspective on distributed antenna systems for the downlink of cellular systems," *IEEE Commun. Mag.*, vol. 51, no. 4, pp. 161–167, Apr. 2013.
- [32] B. Sainath and N. B. Mehta, "Generalizing the amplify-and-forward relay gain model: An optimal SEP perspective," *IEEE Trans. Wireless Commun.*, vol. 11, no. 11, pp. 4118–4127, Nov. 2012.
- [33] J. Huang et al., "Relay beamforming for amplify-and-forward multi-antenna relay networks with energy harvesting constraint," *IEEE Signal Process. Lett.*, vol. 21, no. 4, pp. 454–458, Apr. 2014.
- [34] C. Chae et al., "MIMO relaying with linear processing for multiuser transmission in fixed relay networks," *IEEE Trans. Signal Process.*, vol. 56, no. 2, pp. 727–738, Feb. 2008.
- [35] A. Zappone et al., "Energy efficiency optimization in relay-assisted MIMO systems with perfect and statistical CSI," *IEEE Trans. Signal Process.*, vol. 62, no. 2, pp. 443–457, Jan. 2014.
- [36] N. Kaina et al., "Shaping complex microwave fields in reverberating media with binary tunable metasurfaces," *Sci. Rep.* 4, pp. 1–7, Article No 076401, 2014.
- [37] N. Kaina et al., "Hybridized resonances to design tunable binary phase metasurface unit cells," *Opt. Express*, vol. 22, no. 16, pp. 1–8.

- [38] Q. Wu et al., “Intelligent reflecting surface enhanced wireless network: Joint active and passive beamforming design,” in *Proc. GLOBECOM*, Dec 2018, pp. 1–6.
- [39] L. Subrt and P. Pechac, “Intelligent walls as autonomous parts of smart indoor environments,” *IET Commun.*, vol. 6, no. 8, pp. 1004–1010, May 2012.
- [40] L. Subrt and P. Pechac, “Controlling propagation environments using intelligent walls,” in *Proc. EUCAP*, Prague, Czech Republic, Mar. 2012, pp. 1–5.
- [41] M. Dohler and Y. Li, *Cooperative communications: Hardware, channel & PHY*, Wiley, UK, 2010.
- [42] L. N. Ribeiro et al., “Energy efficiency of mmwave massive MIMO precoding with low-resolution DACs,” *IEEE J. Sel. Topics Signal Process.*, vol. 12, no. 2, pp. 298–312, May 2018.
- [43] R. Méndez-Ria et al., “Hybrid MIMO architectures for millimeter wave communications: Phase shifters or switches?,” *IEEE Access*, vol. 4, pp. 247–267, Jan. 2016.
- [44] C. Huang et al., “Iterative channel estimation using LSE and sparse message passing for mmwave MIMO systems,” *IEEE Trans. Signal Process.*, vol. 67, no. 1, pp. 245–259, Jan 2019.
- [45] S. Wagner et al., “Large system analysis of linear precoding in correlated MISO broadcast channels under limited feedback,” *IEEE Trans. Inf. Theory*, vol. 58, no. 7, pp. 4509–4537, Jul. 2012.
- [46] C. Huang et al., “Asymptotically optimal estimation algorithm for the sparse signal with arbitrary distributions,” *IEEE Trans. on Veh. Tech.*, vol. 67, no. 10, pp. 10070–10075, Oct 2018.
- [47] G. C. Alexandropoulos, “Position aided beam alignment for millimeter wave backhaul systems with large phased arrays,” in *Proc. IEEE CAMSAP*, Curaçao, Dutch Antilles, Dec. 2017, pp. 1–5.
- [48] A. Alkhateeb et al., “Deep learning coordinated beamforming for highly-mobile millimeter wave systems,” [Online] <http://arxiv.org/abs/1804.10334>, 2018.
- [49] I. Csiszár and G. Tusnády, “Information geometry and alternating minimization procedures,” *Statist. Decisions*, vol. 1, pp. 205–237, Dec. 1984.
- [50] L. Tang et al., “Fast algorithms for sparse frequency waveform design with sidelobe constraint,” *Elsevier Digital Signal Process.*, vol. 69, pp. 140–153, 2017.
- [51] P. Stoica et al., “Optimization of the receive filter and transmit sequence for active sensing,” *IEEE Trans. Signal Process.*, vol. 60, no. 4, pp. 1730–1740, Apr. 2012.
- [52] A. Zappone et al., “Globally optimal energy-efficient power control and receiver design in wireless networks,” *IEEE Trans. Signal Process.*, vol. 65, no. 11, pp. 2844–2859, Jun. 2017.
- [53] D. R. Hunter and K. Lange, “A tutorial on MM algorithms,” *American Stat.*, vol. 58, no. 1, pp. 30–37, 2004.
- [54] Y. Sun et al., “Majorization-Minimization algorithms in signal processing, communications, and machine learning,” *IEEE Trans. Signal Process.*, vol. 65, no. 3, pp. 794–816, Feb. 2017.
- [55] J. Song et al., “Optimization methods for designing sequences with low autocorrelation sidelobes,” *IEEE Trans. Signal Process.*, vol. 63, no. 15, pp. 3998–4009, Aug. 2015.
- [56] T. Abrudan et al., “Conjugate gradient algorithm for optimization under unitary matrix constraint,” *Elsevier Signal Process.*, vol. 89, no. 9, pp. 1704–1714, 2009.
- [57] D. Zhao et al., “Spectrum optimization via FFT-based conjugate gradient method for unimodular sequence design,” *Elsevier Signal Process.*, vol. 142, pp. 354–365, 2018.
- [58] J. Liang et al., “Unimodular sequence design based on alternating direction method of multipliers,” *IEEE Trans. Signal Process.*, vol. 64, no. 20, pp. 5367–5381, Oct. 2016.
- [59] C. Huang et al., “Deep learning for UL/DL channel calibration in generic massive MIMO systems large intelligent surfaces,” [Online] <https://arxiv.org/abs/1903.02875>, to appear ICC 2019.

- [60] O. Aldayel et al., “Tractable transmit MIMO beampattern design under a constant modulus constraint,” *IEEE Trans. Signal Process.*, vol. 65, no. 10, pp. 2588–2599, May 2017.
- [61] L. Wu et al., “Cognitive radar-based sequence design via SINR maximization,” *IEEE Trans. Signal Process.*, vol. 65, no. 3, pp. 779–793, Feb. 2017.
- [62] Aharon Ben-Tal and Arkadi Nemirovski, *Lectures on modern convex optimization: analysis, algorithms, and engineering applications*, SIAM, 2001.
- [63] E. Björnson et al., “Optimal design of energy-efficient multi-user MIMO systems: Is massive MIMO the answer?,” *IEEE Trans. Wireless Commun.*, vol. 14, no. 6, pp. 3059–3075, Jun. 2015.
- [64] S. Hu et al., “The potential of positioning with large intelligent surfaces,” *IEEE Trans. Signal Process.*, vol. 66, no. 7, pp. 1761–1774, Apr. 2018.